



THE UNIVERSITY *of* EDINBURGH

Edinburgh Research Explorer

OPEN  ACCESS

Observation of the $B^0 \rightarrow D^0$ decay from an amplitude analysis of $B^0 \rightarrow D^{\pm} K^{\mp}$ decays



Observation of the $B^0 \rightarrow \rho^0 \rho^0$ decay from an amplitude analysis of $B^0 \rightarrow (\pi^+ \pi^-)(\pi^+ \pi^-)$ decays



LHCb Collaboration

ARTICLE INFO

Article history:

Received 26 March 2015

Received in revised form 18 May 2015

Accepted 10 June 2015

Available online 15 June 2015

Editor: M. Doser

ABSTRACT

Proton–proton collision data recorded in 2011 and 2012 by the LHCb experiment, corresponding to an integrated luminosity of 3.0 fb^{-1} , are analysed to search for the charmless $B^0 \rightarrow \rho^0 \rho^0$ decay. More than 600 $B^0 \rightarrow (\pi^+ \pi^-)(\pi^+ \pi^-)$ signal decays are selected and used to perform an amplitude analysis, under the assumption of no CP violation in the decay, from which the $B^0 \rightarrow \rho^0 \rho^0$ decay is observed for the first time with 7.1 standard deviations significance. The fraction of $B^0 \rightarrow \rho^0 \rho^0$ decays yielding a longitudinally polarised final state is measured to be $f_L = 0.745^{+0.048}_{-0.058}(\text{stat}) \pm 0.034(\text{syst})$. The $B^0 \rightarrow \rho^0 \rho^0$ branching fraction, using the $B^0 \rightarrow \phi K^*(892)^0$ decay as reference, is also reported as $\mathcal{B}(B^0 \rightarrow \rho^0 \rho^0) = (0.94 \pm 0.17(\text{stat}) \pm 0.09(\text{syst}) \pm 0.06(\text{BF})) \times 10^{-6}$.

© 2015 CERN for the benefit of the LHCb Collaboration. Published by Elsevier B.V. This is an open access article under the CC BY license (<http://creativecommons.org/licenses/by/4.0/>). Funded by SCOAP³.

1. Introduction

The study of B meson decays to $\rho\rho$ final states provides the most powerful constraint to date for the Cabibbo–Kobayashi–Maskawa (CKM) angle $\alpha \equiv \arg[(V_{td}V_{tb}^*)/(V_{ud}V_{ub}^*)]$ [1–3]. Most of the physics information is provided by the decay $B^0 \rightarrow \rho^+ \rho^-$ as measured at the $e^+ e^-$ colliders at the $\Upsilon(4S)$ resonance [4,5],¹ for which the dominant decay amplitude, involving the emission of a W boson only (tree), exhibits a phase difference that can be interpreted as the sum of the CKM angles $\beta + \gamma = \pi - \alpha$ in the Standard Model. The subleading amplitude associated with the exchange of a W boson and a quark (penguin) must be determined in order to interpret the electroweak phase difference in terms of the angle α . This is realised by means of an isospin analysis involving the companion modes $B^+ \rightarrow \rho^+ \rho^0$ [6,7] and $B^0 \rightarrow \rho^0 \rho^0$ [8,9].² In particular, the smallness of the amplitude of the latter leads to a better constraint on α .

The BaBar and Belle experiments reported evidence for the $B^0 \rightarrow \rho^0 \rho^0$ decay [8,9] with an average branching fraction of $\mathcal{B}(B^0 \rightarrow \rho^0 \rho^0) = (0.97 \pm 0.24) \times 10^{-6}$ [8,9]. Despite small observed signal yields, each experiment measured the fraction f_L of decays yielding a longitudinally polarised final state through an angular analysis. The Belle Collaboration did not find evidence for polarisation, $f_L = 0.21^{+0.22}_{-0.26}$ [9], while the BaBar experiment measured a mostly longitudinally polarised decay, $f_L = 0.75^{+0.12}_{-0.15}$ [8]. These results differ at the level of 2.0 standard deviations. The

large LHCb data set may shed light on this discrepancy. In addition, LHCb may confirm the hint of $B^0 \rightarrow \rho^0 f_0(980)$ decays reported by Belle [9]. Measurements of the $B^0 \rightarrow \rho^0 \rho^0$ branching fraction and longitudinal polarisation fraction at LHCb can be used as inputs in the determination of α [2,3].

This work focuses on the search and study of the $B^0 \rightarrow (\pi^+ \pi^-)(\pi^+ \pi^-)$ decay in which the two $(\pi^+ \pi^-)$ pairs are selected in the low invariant mass range ($< 1100 \text{ MeV}/c^2$). The $B^0 \rightarrow \rho^0 \rho^0$ is expected to dominate the $(\pi^+ \pi^-)$ mass spectrum. The $(\pi^+ \pi^-)$ combinations can actually emerge from S-wave non-resonant and resonant contributions or other P- or D-wave resonances interfering with the signal. Hence, the determination of the $B^0 \rightarrow \rho^0 \rho^0$ yields requires a two-body mass and angular analysis, from which the fraction of the longitudinally polarised final state can be measured.

The branching fraction is measured relative to the $B^0 \rightarrow \phi K^*(892)^0$ mode. The $B^0 \rightarrow \phi K^*(892)^0$ decay, which results in four light mesons in the final state, is similar to the signal, thus allowing for a cancellation of the uncertainties in the ratio of selection efficiencies.

2. Data sets and selection requirements

The analysed data correspond to an integrated luminosity of 1.0 fb^{-1} and 2.0 fb^{-1} from pp collisions recorded at a centre-of-mass energy of 7 TeV , collected in 2011, and 8 TeV , collected in 2012, by the LHCb experiment at CERN.

The LHCb detector [10,11] is a single-arm forward spectrometer covering the pseudorapidity range $2 < \eta < 5$, designed for the study of particles containing b or c quarks. It includes a high-

¹ Charge conjugation is implicit throughout the text unless otherwise stated.

² ρ^0 stands for $\rho^0(770)$ throughout the text.

precision tracking system consisting of a silicon-strip vertex detector surrounding the pp interaction region [12], a large-area silicon-strip detector located upstream of a dipole magnet with a bending power of about 4 Tm, and three stations of silicon-strip detectors and straw drift tubes [13] placed downstream of the magnet. The tracking system provides a measurement of momentum, p , of charged particles with a relative uncertainty that varies from 0.5% at low momentum to 1.0% at 200 GeV/c. The minimum distance of a track to a primary vertex, the impact parameter, is measured with a resolution of $(15 + 29/p_T)$ μm , where p_T is the component of the momentum transverse to the beam, in GeV/c. Different types of charged hadrons are distinguished using information from two ring-imaging Cherenkov (RICH) detectors [14]. Photons, electrons and hadrons are identified by a calorimeter system consisting of scintillating-pad and preshower detectors, an electromagnetic calorimeter and a hadronic calorimeter. Muons are identified by a system composed of alternating layers of iron and multiwire proportional chambers [15]. The online event selection is performed by a trigger [16], which consists of a hardware stage, based on information from the calorimeter and muon systems, followed by a software stage, which applies a full event reconstruction.

In this analysis two categories of events that pass the hardware trigger stage are considered: those where the trigger decision is satisfied by the signal b -hadron decay products (TOS) and those where only the other activity in the event determines the trigger decision (TIS). The software trigger requires a two-, three- or four-track secondary vertex with large transverse momenta of charged particles and a significant displacement from the primary pp interaction vertices (PVs). At least one charged particle should have $p_T > 1.7$ GeV/c and is required to be inconsistent with originating from any primary interaction. A multivariate algorithm [17] is used for the identification of secondary vertices consistent with the decay of a b hadron.

Further selection criteria are applied offline to reduce the number of background events with respect to the signal. The $(\pi^+\pi^-)$ candidates must have transverse momentum larger than 600 MeV/c, with at least one charged decay product with $p_T > 1000$ MeV/c. The two $(\pi^+\pi^-)$ pairs are then combined to form a B^0 candidate with a good vertex quality and transverse momentum larger than 2500 MeV/c. The invariant mass of each pair of opposite-charge pions forming the B^0 candidate is required to be in the range 300–1100 MeV/ c^2 . The identification of the final-state particles (PID) is performed with dedicated neural-networks-based discriminating variables that combine information from the RICH detectors and other properties of the event [14]. The combinatorial background is further suppressed with multivariate discriminators based on a boosted decision tree algorithm (BDT) [18,19]. The BDT is trained with simulated $B^0 \rightarrow \rho^0 \rho^0$ (where $\rho^0 \rightarrow \pi^+\pi^-$) events as signal sample and candidates reconstructed with four-body mass in excess of 5420 MeV/ c^2 as background sample. The discriminating variables are based on the kinematics of the B decay candidate (B p_T and the minimum p_T of the two ρ^0 candidates) and on geometrical vertex measurements (quality of the B candidate vertex, impact parameter significances of the daughters, B flight distance significance and B pointing to the primary vertex). The optimal thresholds for the BDT and PID discriminating variables are determined simultaneously by means of a frequentist estimator for which no hypothesis on the signal yield is assumed [20]. The B^0 meson candidates are accepted in the mass range 5050–5500 MeV/ c^2 .

The normalisation mode $B^0 \rightarrow \phi K^*(892)^0$ is selected with similar criteria, requiring in addition that the invariant mass of the $(K^+\pi^-)$ candidate is found in a range of ± 150 MeV/ c^2 around the known value of the $K^*(892)^0$ meson mass [21] and the invariant mass of the (K^+K^-) pair is in a range of ± 15 MeV/ c^2 centred

at the known value of the ϕ meson mass [21]. A sample enriched in $B^0 \rightarrow (K^+\pi^-)(\pi^+\pi^-)$ events is selected using the same ranges in $(\pi^+\pi^-)$ and $(K^+\pi^-)$ masses to estimate the background with one misidentified kaon.

The presence of $(\pi^+\pi^-)$ pairs originating from J/ψ , χ_{c0} and χ_{c2} charmonia decays is vetoed by requiring the invariant masses M of all possible $(\pi^+\pi^-)$ pairs to be $|M - M_0| > 30$ MeV/ c^2 , where M_0 stands for the corresponding known values of the J/ψ , χ_{c0} and χ_{c2} meson masses [21]. Similarly, the decays $D^0 \rightarrow K^-\pi^+$ and $D^0 \rightarrow \pi^+\pi^-$ are vetoed by requiring the corresponding invariant masses to differ by 25 MeV/ c^2 or more from the known D^0 meson mass [21]. To reduce contamination from other charm backgrounds and from the $B^0 \rightarrow a_1^+(\rightarrow \rho^0\pi^+)\pi^-$ decay, the invariant mass of any three-body combination in the event is required to be larger than 2100 MeV/c 2 .

Simulated $B^0 \rightarrow \rho^0 \rho^0$ and $B^0 \rightarrow \phi K^*(892)^0$ decays are also used for determining the relative reconstruction efficiencies. The pp collisions are generated using PYTHIA [22] with a specific LHCb configuration [23]. Decays of hadronic particles are described by EvtGEN [24]. The interaction of the generated particles with the detector and its response are implemented using the GEANT4 toolkit [25] as described in Ref. [26].

3. Four-body mass fit

The four-body mass spectrum $M(\pi^+\pi^-)(\pi^+\pi^-)$ is fit with an unbinned extended likelihood. The fit is performed simultaneously for the two data taking periods together with the normalisation channel $M(K^+K^-)(K^+\pi^-)$ and PID misidentification control channel $M(K^+\pi^-)(\pi^+\pi^-)$ mass spectra. The four-body invariant mass models account for B^0 and possible B_s^0 signals, combinatorial backgrounds, signal cross-feeds and background contributions arising from partially reconstructed b -hadron decays in which one or more particles are not reconstructed.

The B^0 and B_s^0 meson shapes are modelled with a modified Crystal Ball distribution [27]. A second power-law tail is added on the high-mass side of the signal shape to account for imperfections of the tracking system. The model parameters are determined from a simultaneous fit of simulated signal events that fulfil the trigger, reconstruction and selection chain, for each data taking period. The values of the tail parameters are identical for the B^0 and B_s^0 mesons. Their mass difference is constrained to the value from Ref. [21]. The mean and width of the modified Crystal Ball function are free parameters of the fit to the data.

The combinatorial background in each four-body spectrum is described by an exponential function where the slope is allowed to vary in the fit.

The misidentification of one or more final-state hadrons may result in a fully reconstructed background contribution to the corresponding signal spectrum, denoted signal cross-feed. The magnitude of the branching fractions of the signal and control modes as well as the two-body mass selection criteria make these signal cross-feeds negligible, with one exception: the misidentification of the kaon of the decay $B^0 \rightarrow (K^+\pi^-)(\pi^+\pi^-)$ as a pion yields a significant contribution in the $M(\pi^+\pi^-)(\pi^+\pi^-)$ mass spectrum. The mass shape of $B^0 \rightarrow (K^+\pi^-)(\pi^+\pi^-)$ decays reconstructed as $B^0 \rightarrow (\pi^+\pi^-)(\pi^+\pi^-)$ is modelled by a Crystal Ball function, whose parameters are determined from simulated events. The yield of this signal cross-feed is allowed to vary in the fit. The measurement of the actual number of reconstructed $B^0 \rightarrow (K^+\pi^-)(\pi^+\pi^-)$ events multiplied by the data-driven estimate of the misidentification efficiency is consistent with the measured yield.

The partially reconstructed background is modelled by an ARGUS function [28] convolved with a Gaussian function accounting

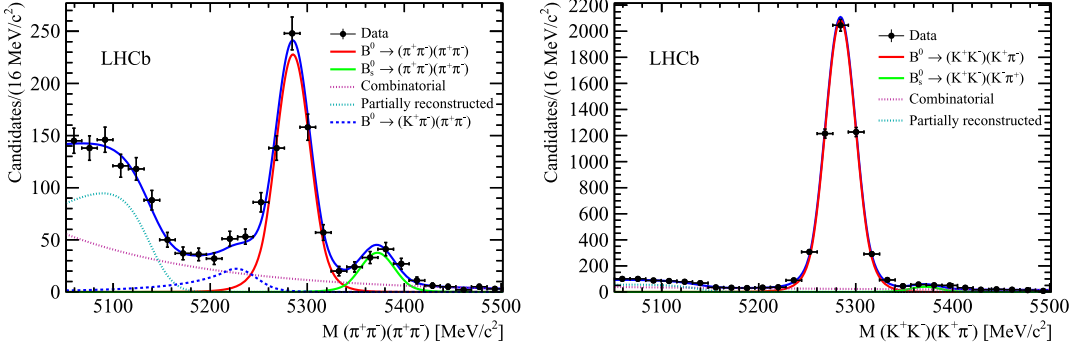


Fig. 1. Reconstructed invariant mass spectrum of (left) $(\pi^+\pi^-)(\pi^+\pi^-)$ and (right) $(K^+K^-)(K^+\pi^-)$. The data are represented by the black dots. The fit is represented by the solid blue line, the B^0 signal by the solid red line and the B_s^0 by the solid green line. The combinatorial background is represented by the pink dotted line, the partially reconstructed background by the cyan dotted line and the cross-feed by the dark blue dashed line. (For interpretation of the references to colour in this figure legend, the reader is referred to the web version of this article.)

Table 1

Yields from the simultaneous fit for the 2011 and 2012 data sets. The first and second uncertainties are the statistical and systematic contributions, respectively.

Decay mode	Signal yields 2011	Signal yields 2012
$B^0 \rightarrow (\pi^+\pi^-)(\pi^+\pi^-)$	$185 \pm 15 \pm 4$	$449 \pm 24 \pm 7$
$B^0 \rightarrow (K^+\pi^-)(\pi^+\pi^-)$	$1610 \pm 42 \pm 5$	$3478 \pm 62 \pm 10$
$B^0 \rightarrow (K^+K^-)(K^+\pi^-)$	$1513 \pm 40 \pm 8$	$3602 \pm 62 \pm 10$
$B_s^0 \rightarrow (\pi^+\pi^-)(\pi^+\pi^-)$	$30 \pm 7 \pm 1$	$71 \pm 11 \pm 1$
$B_s^0 \rightarrow (K^-\pi^+)(\pi^+\pi^-)$	$40 \pm 10 \pm 3$	$96 \pm 14 \pm 6$
$B_s^0 \rightarrow (K^+K^-)(K^-\pi^+)$	$42 \pm 10 \pm 3$	$66 \pm 13 \pm 4$

for resolution effects. Various mass shape parameterisations are examined. The best fit is obtained when the endpoint of the ARGUS function is fixed to the value expected when one pion is not attributed to the decay. The other shape parameters of the ARGUS function are free parameters of the fit, common to the two data taking periods. The floating width parameter of the signal mass shape is constrained to be equal to the width of the Gaussian function used in the convolution.

Fig. 1 displays the $M(\pi^+\pi^-)(\pi^+\pi^-)$ and $M(K^+K^-)(K^+\pi^-)$ spectra with the fit results overlaid. The signal event yields are shown in Table 1. Aside from the prominent signal of the $B^0 \rightarrow (\pi^+\pi^-)(\pi^+\pi^-)$ decays, the decay mode $B_s^0 \rightarrow (\pi^+\pi^-)(\pi^+\pi^-)$ is observed with a statistical significance of more than 10 standard deviations. The statistical significance is evaluated by taking the ratio of the likelihood of the nominal fit and of the fit with the signal yield fixed to zero.

A systematic uncertainty due to the fit model is associated to the measured yields. The dominant uncertainties arise from the knowledge of the signal and signal cross-feed shape parameters determined from simulated events. Several pseudoexperiments are generated while varying the shape parameters within their uncertainties, and the systematic uncertainties on the yields are estimated from the differences in results with respect to the nominal fit.

4. Amplitude analysis

An amplitude analysis is used to determine the vector–vector (VV) contribution $B^0 \rightarrow \rho^0 \rho^0$ by using two-body mass spectra and angular variables. The four-body mass spectrum is first analysed with the *sPlot* technique [29] to subtract statistically the background under the $B^0 \rightarrow (\pi^+\pi^-)(\pi^+\pi^-)$ signal.

For the two-body mass spectra, contributions from resonant and non-resonant scalar (S), resonant vector (V) and tensor (T) components are considered in the amplitude fit model through complex mass propagators, $M(m_i)$, where the label $i = 1, 2$ are the

first and second pion pairs, which are assigned randomly in every decay since they are indistinguishable. The P-wave lineshape model comprises the ρ^0 meson, described using the Gounaris–Sakurai parameterisation $M_\rho(m_i)$ [30], and the ω meson, parameterised with a relativistic spin-1 Breit–Wigner $M_\omega(m_i)$. The D-wave lineshape $M_{f_2}(m_i)$ accounts for the $f_2(1270)$, modelled with a relativistic spin-2 Breit–Wigner. The S-wave model includes the $f_0(980)$ propagator $M_{f(980)}(m_i)$, described using a Flatté parameterisation [31,32], and a low-mass component. The latter includes the broad low-mass resonance $f_0(500)$ and a non-resonant contributions, which are jointly modelled in the framework of the K -matrix formalism [33] and referred as $M_{(\pi\pi)_0}(m_i)$. Following the K -matrix formalism, the amplitude for the low-mass $\pi^+\pi^-$ S-wave can be written as

$$A(m) \propto \frac{\hat{K}}{1 - i\rho\hat{K}}, \quad (1)$$

with

$$\hat{K} \equiv \hat{K}_{\text{res}} + \hat{K}_{\text{non-res}} = \frac{m_0\Gamma(m)}{(m_0^2 - m^2)\rho(m)} + \kappa, \quad (2)$$

$$\rho(m) = 2 \left(\frac{q(m)}{m} \right), \quad (3)$$

where κ is measured to be -0.07 ± 0.24 from a fit to the inclusive $\pi^+\pi^-$ mass distribution and m_0 and Γ are the nominal mass and mass-dependent width of the $f_0(500)$, as determined in Ref. [34]. The functions $\rho(m)$ and $q(m)$, defined in Ref. [33], are the phase space factor and the relative momentum of a pion in the ρ^0 centre-of-mass system. By convention, the phase of the $M_{(\pi\pi)_0}(m_i)$ mass propagator is set to zero at the ρ^0 nominal mass.

The signal sample is described by considering the dominant amplitudes of the signal decay. The $B \rightarrow VV$ component contains the $B \rightarrow \rho^0 \rho^0$ and $B^0 \rightarrow \rho^0 \omega$ amplitudes. The $B \rightarrow VS$ component accounts for $B^0 \rightarrow \rho^0(\pi^+\pi^-)_0$ and $B^0 \rightarrow \rho^0 f_0(980)$ amplitudes and the $B \rightarrow VT$ contribution is limited to the purely longitudinal amplitude of the $B^0 \rightarrow \rho^0 f_2(1270)$ transition. Because of the broad natural width of the a_1^\pm particle, a small contamination from the decays $B^0 \rightarrow a_1^\pm \pi^\mp$ remains in the sample. This contribution with $a_1^\pm \rightarrow \rho^0 \pi^\pm$ in S-wave is considered along with its interference with the other amplitudes. This is done by introducing the CP -even eigenstate from the linear combination of individual amplitudes of the decays $B^0 \rightarrow a_1^+ \pi^-$ and $B^0 \rightarrow a_1^- \pi^+$, as defined in Ref. [35]. The contribution of the decays $B^0 \rightarrow \omega\omega$, $B^0 \rightarrow f_0(980)f_0(980)$, $B^0 \rightarrow \omega S$, $B^0 \rightarrow \omega T$, $B^0 \rightarrow f_2(1270)S$, $B^0 \rightarrow f_2(1270)f_2(1270)$ and $B^0 \rightarrow (\rho^0 f_2(1270))_{\parallel,\perp}$ are assumed

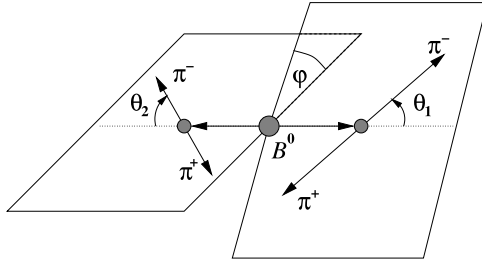


Fig. 2. Helicity angles for the $(\pi^+\pi^-)(\pi^+\pi^-)$ system.

to be negligible, where the \parallel and \perp subindices indicate the parallel and perpendicular amplitudes of the decay. The choice of the baseline model was made prior to the measurement of the physical parameters of interest after comparing a set of alternative parameterisations according to a dissimilarity statistical test [36].

The differential decay rate for $B^0 \rightarrow (\pi^+\pi^-)(\pi^+\pi^-)$ decays at the B^0 production time $t = 0$ is given by

$$\frac{d^5\Gamma}{d\cos\theta_1 d\cos\theta_2 d\varphi dm_1^2 dm_2^2} \propto \Phi_4(m_1, m_2) \left| \sum_{i=1}^{11} A_i f_i(m_1, m_2, \theta_1, \theta_2, \varphi) \right|^2, \quad (4)$$

where the variables θ_1 , θ_2 and φ are the helicity angles, described in Fig. 2, and Φ_4 is the four-body phase space factor. The notations of the complex amplitudes, A_i , and the expressions of their related angular distributions, f_i , are displayed in Table 2. The mass propagators included in the f_i functions are normalised to unity in the fit range.

For the CP conjugated mode, $\bar{B}^0 \rightarrow (\pi^+\pi^-)(\pi^+\pi^-)$, the decay rate is obtained under the transformation $A_i \rightarrow \eta_i \bar{A}_i$, where η_i is the CP eigenvalue of the CP eigenstate i , shown in Table 2.

The untagged time-integrated decay rate of B^0 and \bar{B}^0 to four pions, assuming no CP violation, can be written as

$$\frac{d^5(\Gamma + \bar{\Gamma})}{d\cos\theta_1 d\cos\theta_2 d\varphi dm_1^2 dm_2^2} \propto \sum_{j=1}^{11} \sum_{i \leq j} \mathcal{R}e[A_i A_j^* f_i f_j^*] (2 - \delta_{ij}) (1 + \eta_i \eta_j) \Phi_4(m_1, m_2), \quad (5)$$

where $\delta_{ij} = 1$ when $i = j$ and $\delta_{ij} = 0$ otherwise.

Table 2

Amplitudes, A_i , CP eigenvalues, η_i , and mass-angle distributions, f_i , of the $B^0 \rightarrow (\pi^+\pi^-)(\pi^+\pi^-)$ model. The indices $ijkl$ indicate the eight possible combinations of pairs of opposite-charge pions. The angles α_{kl} , β_{ij} and Φ_{kl} are defined in Ref. [37].

A_i	η_i	f_i
$A_{\rho\rho}^0$	1	$M_\rho(m_1)M_\rho(m_2)\cos\theta_1\cos\theta_2$
$A_{\rho\rho}^\parallel$	1	$M_\rho(m_1)M_\rho(m_2)\frac{1}{\sqrt{2}}\sin\theta_1\sin\theta_2\cos\varphi$
$A_{\rho\rho}^\perp$	-1	$M_\rho(m_1)M_\rho(m_2)\frac{1}{\sqrt{2}}\sin\theta_1\sin\theta_2\sin\varphi$
$A_{\rho\omega}^0$	1	$\frac{1}{\sqrt{2}}[M_\rho(m_1)M_\omega(m_2) + M_\omega(m_1)M_\rho(m_2)]\cos\theta_1\cos\theta_2$
$A_{\rho\omega}^\parallel$	1	$\frac{1}{\sqrt{2}}[M_\rho(m_1)M_\omega(m_2) + M_\omega(m_1)M_\rho(m_2)]\frac{1}{\sqrt{2}}\sin\theta_1\sin\theta_2\cos\varphi$
$A_{\rho\omega}^\perp$	-1	$\frac{1}{\sqrt{2}}[M_\rho(m_1)M_\omega(m_2) + M_\omega(m_1)M_\rho(m_2)]\frac{1}{\sqrt{2}}\sin\theta_1\sin\theta_2\sin\varphi$
$A_{\rho(\pi\pi)_0}$	-1	$\frac{1}{\sqrt{6}}[M_\rho(m_1)M_{(\pi\pi)_0}(m_2)\cos\theta_1 + M_{(\pi\pi)_0}(m_1)M_\rho(m_2)\cos\theta_2]$
$A_{\rho f(980)}$	-1	$\frac{1}{\sqrt{6}}[M_\rho(m_1)M_{f(980)}(m_2)\cos\theta_1 + M_{f(980)}(m_1)M_\rho(m_2)\cos\theta_2]$
$A_{(\pi\pi)_0(\pi\pi)_0}$	1	$M_{(\pi\pi)_0}(m_1)M_{(\pi\pi)_0}(m_2)\frac{1}{3}$
$A_{\rho f_2}^0$	-1	$\sqrt{\frac{5}{24}}[M_\rho(m_1)M_{f_2}(m_2)\cos\theta_1(3\cos^2\theta_2 - 1) + M_{f_2}(m_1)M_\rho(m_2)\cos\theta_2(3\cos^2\theta_1 - 1)]$
$A_{a_1\pi}^{S^+}$	1	$\frac{1}{\sqrt{8}}\sum_{ijkl}\frac{1}{\sqrt{3}}M_{a_1}(m_{ijk})M_\rho(m_{ij})[\cos\alpha_{kl}\cos\beta_{ik} + \sin\alpha_{kl}\sin\beta_{ik}\cos\Phi_{kl}]$

The efficiency of the selection of the final state $B^0 \rightarrow (\pi^+\pi^-)(\pi^+\pi^-)$ varies as a function of the helicity angles and the two-body invariant masses. To take into account variations in the efficiencies, four event categories k are defined according to their hardware trigger decisions (TIS or TOS) and data taking period (2011 and 2012).

The acceptance is accounted for through the complex integrals

$$\omega_{ij}^k = \int \epsilon(\theta_1, \theta_2, \varphi, m_1, m_2) f_i f_j^* (2 - \delta_{ij}) \times \Phi_4(m_1, m_2) d\cos\theta_1 d\cos\theta_2 d\varphi dm_1^2 dm_2^2, \quad (6)$$

where f_i are the functions given in Table 2 and ϵ the overall efficiency. The integrals are computed with simulated events of each of the four considered categories, selected with the same criteria as those applied to data, following the method described in Ref. [38]. The coefficients ω_{ij}^k are used to determine the efficiency and to build a probability density function for each category, which is defined as

$$\begin{aligned} S^k(m_1, m_2, \theta_1, \theta_2, \varphi) \\ = \frac{\sum_{j=1}^{11} \sum_{i \leq j} \mathcal{R}e[A_i A_j^* f_i f_j^*] (2 - \delta_{ij}) (1 + \eta_i \eta_j) \Phi_4(m_1, m_2)}{\sum_{j=1}^{11} \sum_{i \leq j} \mathcal{R}e[A_i A_j^* \omega_{ij}^k] (1 + \eta_i \eta_j)}. \end{aligned} \quad (7)$$

The four event categories are used in the simultaneous unbinned maximum likelihood fit which depends on the 19 free parameters indicated in Table 3.

Systematic effects are estimated by fitting with the angular model and ensemble of 1000 pseudoexperiments generated with the same number of events as observed in data. The biases are for the parameters of interest consistent with zero. A systematic uncertainty is assigned by taking 50% of the fit bias or the uncertainty on the rms when the latter is bigger in order to account for possible statistical fluctuations.

Several model related uncertainties are envisaged. The $B^0 \rightarrow a_1^\pm \pi^\mp$ angular model requires knowledge of the lineshape of the a_1^\pm meson. The a_1^\pm natural width is chosen to be 400 MeV/c². The difference to the fit results obtained by varying the width from 250 to 600 MeV/c² is taken as the corresponding systematic uncertainty. In addition, a systematic uncertainty is obtained by introducing the CP -odd component in the fit model of the decay amplitude $B^0 \rightarrow a_1^\pm \pi^\mp$ by fixing the relative amplitudes of $B^0 \rightarrow a_1^+ \pi^-$ and $B^0 \rightarrow a_1^- \pi^+$ components to the values measured in Ref. [39].

Table 3

Results of the unbinned maximum likelihood fit to the angular and two-body invariant mass distributions. The first uncertainty is statistical, the second systematic.

Parameter	Definition	Fit result
f_L	$ A_{\rho\rho}^0 ^2/(A_{\rho\rho}^0 ^2 + A_{\rho\rho}^\parallel ^2 + A_{\rho\rho}^\perp ^2)$	$0.745^{+0.048}_{-0.058} \pm 0.034$
f'_\parallel	$ A_{\rho\rho}^\parallel ^2/(A_{\rho\rho}^\parallel ^2 + A_{\rho\rho}^\perp ^2)$	$0.50 \pm 0.09 \pm 0.05$
$\delta_\parallel - \delta_0$	$\arg(A_{\rho\rho}^\parallel A_{\rho\rho}^{0*})$	$1.84 \pm 0.20 \pm 0.14$
$F_{\rho(\pi\pi)_0}$	$ A_{\rho(\pi\pi)_0} ^2/(A_{\rho\rho}^0 ^2 + A_{\rho\rho}^\parallel ^2 + A_{\rho\rho}^\perp ^2)$	$0.30^{+0.11}_{-0.09} \pm 0.08$
$F_{\rho f(980)}$	$ A_{\rho f(980)} ^2/(A_{\rho\rho}^0 ^2 + A_{\rho\rho}^\parallel ^2 + A_{\rho\rho}^\perp ^2)$	$0.29^{+0.12}_{-0.09} \pm 0.08$
$F_{(\pi\pi)_0(\pi\pi)_0}$	$ A_{(\pi\pi)_0(\pi\pi)_0} ^2/(A_{\rho\rho}^0 ^2 + A_{\rho\rho}^\parallel ^2 + A_{\rho\rho}^\perp ^2)$	$0.21^{+0.06}_{-0.04} \pm 0.08$
$\delta_\perp - \delta_{\rho(\pi\pi)_0}$	$\arg(A_{\rho\rho}^\perp A_{\rho(\pi\pi)_0}^*)$	$-1.13^{+0.33}_{-0.22} \pm 0.24$
$\delta_\perp - \delta_{\rho f(980)}$	$\arg(A_{\rho\rho}^\perp A_{\rho f(980)}^*)$	$1.92 \pm 0.24 \pm 0.16$
$\delta_{(\pi\pi)_0(\pi\pi)_0} - \delta_0$	$\arg(A_{(\pi\pi)_0(\pi\pi)_0} A_{\rho\rho}^{0*})$	$3.14^{+0.36}_{-0.38} \pm 0.39$
$F_{\rho\omega}$	$(A_{\rho\omega}^0 ^2 + A_{\rho\omega}^\parallel ^2 + A_{\rho\omega}^\perp ^2)/(A_{\rho\rho}^0 ^2 + A_{\rho\rho}^\parallel ^2 + A_{\rho\rho}^\perp ^2)$	$0.025^{+0.048}_{-0.022} \pm 0.020$
$f_L^{\rho\omega}$	$ A_{\rho\omega}^0 ^2/(A_{\rho\omega}^0 ^2 + A_{\rho\omega}^\parallel ^2 + A_{\rho\omega}^\perp ^2)$	$0.70^{+0.23}_{-0.60} \pm 0.13$
$f_\parallel^{\rho\omega'}$	$ A_{\rho\omega}^\parallel ^2/(A_{\rho\omega}^\parallel ^2 + A_{\rho\omega}^\perp ^2)$	$0.97^{+0.69}_{-0.56} \pm 0.15$
$\delta_0^\omega - \delta_0$	$\arg(A_{\rho\omega}^0 A_{\rho\rho}^{0*})$	$-2.56^{+0.76}_{-0.92} \pm 0.22$
$\delta_\parallel^\omega - \delta_0$	$\arg(A_{\rho\omega}^\parallel A_{\rho\rho}^{0*})$	$-0.71^{+0.71}_{-0.67} \pm 0.32$
$\delta_\perp^\omega - \delta_{\rho(\pi\pi)_0}$	$\arg(A_{\rho\omega}^\perp A_{\rho(\pi\pi)_0}^*)$	$-1.72 \pm 2.62 \pm 0.80$
$F_{\rho f_2}^0$	$ A_{\rho f_2}^0 ^2/(A_{\rho\rho}^0 ^2 + A_{\rho\rho}^\parallel ^2 + A_{\rho\rho}^\perp ^2)$	$0.01^{+0.04}_{-0.02} \pm 0.03$
$\delta_{\rho f_2}^0 - \delta_{\rho(\pi\pi)_0}$	$\arg(A_{\rho f_2}^0 A_{\rho(\pi\pi)_0}^*)$	$-0.56 \pm 1.48 \pm 0.80$
$F_{a_1\pi}^{S^+}$	$ A_{a_1\pi}^{S^+} ^2/(A_{\rho\rho}^0 ^2 + A_{\rho\rho}^\parallel ^2 + A_{\rho\rho}^\perp ^2)$	$1.4^{+1.0+1.2}_{-0.7-0.8}$
$\delta_{a_1\pi}^{S^+} - \delta_{\rho(\pi\pi)_0}$	$\arg(A_{a_1\pi}^{S^+} A_{\rho(\pi\pi)_0}^*)$	$-0.09^{+0.30}_{-0.36} \pm 0.38$

Another source of uncertainty originates in the modelling of the low mass ($\pi^+\pi^-$) S-wave lineshape. The $f_0(500)$ mass and natural width uncertainties from Ref. [34] and the uncertainty on the parameter that quantifies the non-resonant contribution are propagated to the angular analysis parameters by generating and fitting 1000 pseudoexperiments in which these input values are varied according to a Gaussian distribution having their uncertainties as widths. The root mean square of the distribution of the results is assigned as a systematic uncertainty. The same strategy is followed to estimate the systematic uncertainties originating from the ρ^0 , $f_0(500)$ and ω lineshape parameters.

The uncertainty related to the background subtraction method is estimated by varying within their uncertainties the fixed parameters of the mass fit model and studying the resulting angular distributions and two-body mass spectra. The difference to the fit results is taken as a systematic uncertainty. An alternative subtraction of the background estimated from the high-mass sideband is performed, yielding compatible results.

The knowledge of the acceptance model described in Eq. (6) comes from a finite sample of simulated events. An ensemble of pseudoexperiments is generated by varying the acceptance weights according to their covariance matrix. The root mean square of the distribution of the results is assigned as a systematic uncertainty.

The resolution on the helicity angles is evaluated with pseudoexperiments resulting in a negligible systematic uncertainty. The systematic uncertainty related to the ($\pi^+\pi^-$) mass resolution is estimated with pseudoexperiments by introducing a smearing of the ($\pi^+\pi^-$) mass. Differences in the parameters between the fit with and without smearing are taken as a systematic uncertainty.

Table 4 details the contributions to the systematic uncertainty in the measurement of the fraction of $B^0 \rightarrow \rho^0 \rho^0$ signal decays in the $B^0 \rightarrow (\pi^+\pi^-)(\pi^+\pi^-)$ and its longitudinal polarisation fraction.

The final results of the combined two-body mass and angular analysis are shown in Fig. 3 and Table 3. The fit also allows for

Table 4

Relative systematic uncertainties on the longitudinal polarisation parameter, f_L , and the fraction of $B^0 \rightarrow \rho^0 \rho^0$ decays in the $B^0 \rightarrow (\pi^+\pi^-)(\pi^+\pi^-)$ sample. The model uncertainty includes the three uncertainties below.

Systematic effect	Uncertainty on f_L (%)	Uncertainty on $P(B^0 \rightarrow \rho^0 \rho^0)$ (%)
Fit bias	0.1	0.8
Model	3.6	6.2
$B^0 \rightarrow a_1(1260)^+\pi^-$	1.2	1.1
S-wave lineshape	3.4	6.1
Lineshapes	<0.1	0.1
Background subtraction	0.1	0.5
Acceptance integrals	2.7	4.5
Angular/Mass resolution	0.8	1.5

the extraction of the fraction of $B^0 \rightarrow \rho^0 \rho^0$ decays in the $B^0 \rightarrow (\pi^+\pi^-)(\pi^+\pi^-)$ sample, defined as

$$P(B^0 \rightarrow \rho^0 \rho^0) = \frac{\sum_{j=1}^3 \sum_{i \leq j} \text{Re}[A_i A_j^* \omega_{ij}]}{\sum_{j=1}^{11} \sum_{i \leq j} \text{Re}[A_i A_j^* \omega_{ij}]}, \quad (8)$$

which is

$$P(B^0 \rightarrow \rho^0 \rho^0) = 0.619 \pm 0.072 \text{ (stat)} \pm 0.049 \text{ (syst)}.$$

The $B^0 \rightarrow \rho^0 \rho^0$ signal significance is measured to be 7.1 standard deviations. The significance is obtained by dividing the value of the purity by the quadrature of the statistical and systematic uncertainties. No evidence for the $B^0 \rightarrow \rho^0 f_0(980)$ decay mode is obtained. The fraction of longitudinal polarisation of the $B^0 \rightarrow \rho^0 \rho^0$ decay is measured to be

$$f_L = 0.745^{+0.048}_{-0.058} \text{ (stat)} \pm 0.034 \text{ (syst)}.$$

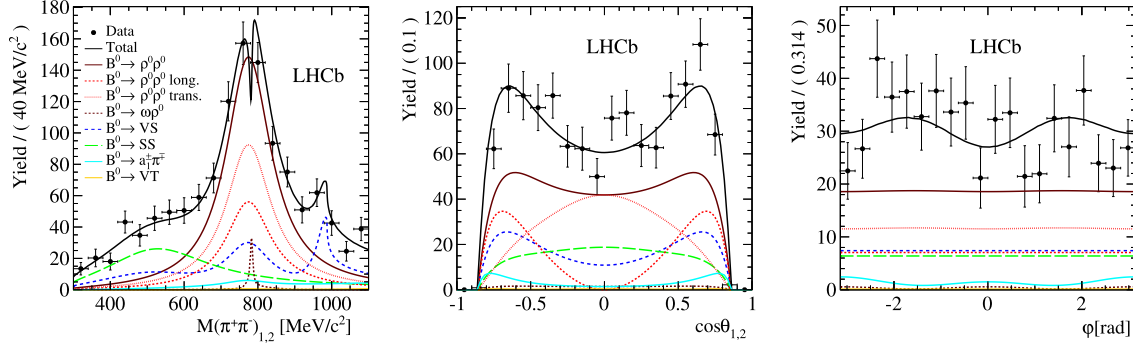


Fig. 3. Background-subtracted $M(\pi^+\pi^-)_{1,2}$, $\cos\theta_{1,2}$ and φ distributions. The black dots correspond to the four-body background-subtracted data and the black line is the projection of the fit model. The specific decays $B^0 \rightarrow \rho^0\rho^0$ (brown), $B^0 \rightarrow \omega\rho^0$ (dashed brown), $B^0 \rightarrow VS$ (dashed blue), $B^0 \rightarrow SS$ (long dashed green), $B^0 \rightarrow VT$ (orange) and $B^0 \rightarrow a_1^\pm\pi^\mp$ (light blue) are also displayed. The $B^0 \rightarrow \rho^0\rho^0$ contribution is split into longitudinal (dashed red) and transverse (dotted red) components. Interference contributions are only plotted for the total (black) model. The efficiency for longitudinally polarised $B^0 \rightarrow \rho^0\rho^0$ events is ~ 5 times smaller than for the transverse component. (For interpretation of the references to colour in this figure legend, the reader is referred to the web version of this article.)

5. Branching fraction determination

The branching fraction of the decay mode $B^0 \rightarrow \rho^0\rho^0$ relative to the decay $B^0 \rightarrow \phi K^*(892)^0$ can be expressed as

$$\begin{aligned} & \frac{\mathcal{B}(B^0 \rightarrow \rho^0\rho^0)}{\mathcal{B}(B^0 \rightarrow \phi K^*(892)^0)} \\ &= \frac{\lambda_{f_L} \cdot P(B^0 \rightarrow \rho^0\rho^0)}{P(B^0 \rightarrow \phi K^*(892)^0)} \times \frac{N'(B^0 \rightarrow (\pi^+\pi^-)(\pi^+\pi^-))}{N'(B^0 \rightarrow (K^+K^-)(K^+\pi^-))} \\ & \quad \times \frac{\mathcal{B}(\phi \rightarrow K^+K^-)\mathcal{B}(K^* \rightarrow K^+\pi^-)}{\mathcal{B}(\rho^0 \rightarrow \pi^+\pi^-)^2}, \end{aligned} \quad (9)$$

where the factor λ_{f_L} corrects for differences in detection efficiencies between experimental and simulated data due to the polarisation hypothesis of the $B^0 \rightarrow \rho^0\rho^0$ sample, $P(B^0 \rightarrow \rho^0\rho^0)$ and $P(B^0 \rightarrow \phi K^*(892)^0)$ are the fractions of $B^0 \rightarrow \rho^0\rho^0$ and $B^0 \rightarrow \phi K^*(892)^0$ signals in the samples of $B^0 \rightarrow (\pi^+\pi^-)(\pi^+\pi^-)$ and $B^0 \rightarrow (K^+K^-)(K^+\pi^-)$ decays, respectively. The quantities $N'(B^0 \rightarrow (\pi^+\pi^-)(\pi^+\pi^-))$ and $N'(B^0 \rightarrow (K^+K^-)(K^+\pi^-))$ are the yields of $B^0 \rightarrow (\pi^+\pi^-)(\pi^+\pi^-)$ and $B^0 \rightarrow (K^+K^-)(K^+\pi^-)$ decays as determined from a fit to the four-body mass distributions, weighted for each data-taking period by the efficiencies of the signal and normalisation channels obtained from their respective simulated data. Finally, $\mathcal{B}(\phi \rightarrow K^+K^-)$, $\mathcal{B}(K^*(892)^0 \rightarrow K^+\pi^-)$ and $\mathcal{B}(\rho^0 \rightarrow \pi^+\pi^-)$ denote known branching fractions [21].

The product $\lambda_{f_L} \cdot P(B^0 \rightarrow \rho^0\rho^0)$ is determined from the amplitude analysis to be 1.13 ± 0.19 (stat) ± 0.10 (syst). This quantity is mainly related to the modelling of the S-wave component, and dominates the systematic uncertainty of the parameters of interest.

The fraction of $B^0 \rightarrow \phi K^*(892)^0$ present in the $B^0 \rightarrow (K^+K^-)(K^+\pi^-)$ sample is taken from Ref. [40]. A 1% systematic uncertainty is added, accounting for differences in the selection acceptance for P- and S-wave contributions.

The amounts of $B^0 \rightarrow (\pi^+\pi^-)(\pi^+\pi^-)$ and $B^0 \rightarrow (K^+K^-)(K^+\pi^-)$ candidates are determined from the four-body mass spectra analysis and their associated statistical and systematical uncertainties are propagated quadratically to the branching fraction uncertainty estimate.

The limited size of the simulated events samples that meet all selection criteria result in a systematic uncertainty of 1.7% (2.6%) on the measurement of the relative branching fraction for the 2011 (2012) data-taking period. The impact of the discrepancies between experimental and simulated data related to the B^0 meson kinematical properties is 0.6% (1.2%). The efficiencies of the particle-identification requirements are determined from control

samples of data with a systematic uncertainty of 0.5%, mostly originating from the limited size of the calibration samples. An additional 1% systematic uncertainty on the tracking efficiency is added accounting for different interaction lengths between π and K .

The relative branching fraction is measured to be

$$\frac{\mathcal{B}(B^0 \rightarrow \rho^0\rho^0)}{\mathcal{B}(B^0 \rightarrow \phi K^*(892)^0)} = 0.094 \pm 0.017 \text{ (stat)} \pm 0.009 \text{ (syst)}. \quad (10)$$

The agreement between the results obtained in the two data-taking periods is tested with the best linear estimator technique [41] yielding compatible results.

The average branching fraction of $B^0 \rightarrow \phi K^*(892)^0$ as determined in Ref. [21] does not take into account the correlations between systematic uncertainties due to the S-wave modelling. Instead, we average the results from Refs. [42–44] including these correlations to obtain $\mathcal{B}(B^0 \rightarrow \phi K^*(892)^0) = (1.00 \pm 0.04 \pm 0.05) \times 10^{-5}$. Using this value in Eq. (10), the branching fraction of $B^0 \rightarrow \rho^0\rho^0$ is

$$\begin{aligned} & \mathcal{B}(B^0 \rightarrow \rho^0\rho^0) \\ &= (0.94 \pm 0.17 \text{ (stat)} \pm 0.09 \text{ (syst)} \pm 0.06 \text{ (BF)}) \times 10^{-6}, \end{aligned}$$

where the last uncertainty is due to the normalisation channel branching fraction. Using the $B^0 \rightarrow \rho^0\rho^0$ branching fraction, the $\rho^0 f_0(980)$ amplitude, a phase space correction and assuming 100% correlated uncertainties, an upper limit for the $B^0 \rightarrow \rho^0 f_0(980)$ decay, at 90% confidence level, is obtained

$$\mathcal{B}(B^0 \rightarrow \rho^0 f_0(980)) \times \mathcal{B}(f_0(980) \rightarrow \pi^+\pi^-) < 0.81 \times 10^{-6}. \quad (11)$$

6. Conclusions

The full data set collected by the LHCb experiment in 2011 and 2012, corresponding to an integrated luminosity of 3.0 fb^{-1} , is analysed to search for the $B^0 \rightarrow \rho^0\rho^0$ decay. A yield of $634 \pm 28 \pm 8$ $B^0 \rightarrow (\pi^+\pi^-)(\pi^+\pi^-)$ signal decays with $\pi^+\pi^-$ pairs in the $300\text{--}1100 \text{ MeV}/c^2$ mass range is obtained. An amplitude analysis is conducted to determine the contribution from $B^0 \rightarrow \rho^0\rho^0$ decays. This decay mode is observed for the first time with a significance of 7.1 standard deviations. In the same $\pi^+\pi^-$ pairs mass range, $B_s^0 \rightarrow (\pi^+\pi^-)(\pi^+\pi^-)$ decays are also observed with a statistical significance of more than 10 standard deviations.

The longitudinal polarisation fraction of the $B^0 \rightarrow \rho^0\rho^0$ decay is measured to be $f_L = 0.745^{+0.048}_{-0.058}$ (stat) ± 0.034 (syst). The measurement of the $B^0 \rightarrow \rho^0\rho^0$ branching fraction reads

$$\mathcal{B}(B^0 \rightarrow \rho^0 \rho^0) = (0.94 \pm 0.17 \text{ (stat)} \pm 0.09 \text{ (syst)} \pm 0.06 \text{ (BF)}) \times 10^{-6},$$

where the last uncertainty is due to the normalisation channel. These results are the most precise to date and will improve the precision of the determination of the CKM angle α .

The measured longitudinal polarisation fraction is consistent with the measured value from BaBar [8] while it differs by 2.3 standard deviations from the value obtained by Belle [9]. The branching fraction measurement is in agreement with the values measured by both BaBar [8] and Belle [9] Collaborations.

The evidence of the $B^0 \rightarrow \rho^0 f_0(980)$ decay mode reported by the Belle Collaboration [9] is not confirmed, and an upper limit at 90% confidence level is established

$$\mathcal{B}(B^0 \rightarrow \rho^0 f_0(980)) \times \mathcal{B}(f_0(980) \rightarrow \pi^+ \pi^-) < 0.81 \times 10^{-6}.$$

Acknowledgements

We express our gratitude to our colleagues in the CERN accelerator departments for the excellent performance of the LHC. We thank the technical and administrative staff at the LHCb institutes. We acknowledge support from CERN and from the national agencies: CAPES, CNPq, FAPERJ and FINEP (Brazil); NSFC (China); CNRS/IN2P3 (France); BMBF, DFG, HGF and MPG (Germany); INFN (Italy); FOM and NWO (The Netherlands); MNiSW and NCN (Poland); MEN/IFA (Romania); MINES and FANO (Russia); MinECo (Spain); SNSF and SER (Switzerland); NASU (Ukraine); STFC (United Kingdom); NSF (USA). The Tier1 computing centres are supported by IN2P3 (France), KIT and BMBF (Germany), INFN (Italy), NWO and SURF (The Netherlands), PIC (Spain), GridPP (United Kingdom). We are indebted to the communities behind the multiple open source software packages on which we depend. We are also thankful for the computing resources and the access to software R&D tools provided by Yandex LLC (Russia). Individual groups or members have received support from EPLANET, Marie Skłodowska-Curie Actions and ERC (European Union), Conseil général de Haute-Savoie, Labex ENIGMASS and OCEVU, Région Auvergne (France), RFBR (Russia), XuntaGal and GENCAT (Spain), Royal Society and Royal Commission for the Exhibition of 1851 (United Kingdom).

References

- [1] M. Gronau, D. London, Isospin analysis of CP asymmetries in B decays, Phys. Rev. Lett. 65 (1990) 3381.
- [2] J. Charles, et al., Current status of the Standard Model CKM fit and constraints on $\Delta F = 2$ new physics, arXiv:1501.5013.
- [3] A. Bevan, et al., Standard model updates and new physics analysis with the unitarity triangle fit, Nucl. Phys. Proc. Suppl. 241–242 (2013) 89.
- [4] BaBar Collaboration, B. Aubert, et al., A study of $B^0 \rightarrow \rho^+ \rho^-$ decays and constraints on the CKM angle alpha, Phys. Rev. D 76 (2007) 052007, arXiv:0705.2157.
- [5] Belle Collaboration, A. Somov, et al., Improved measurement of CP-violating parameters in $B^0 \rightarrow \rho^+ \rho^-$ decays, Phys. Rev. D 76 (2007) 011104, arXiv:hep-ex/0702009.
- [6] Belle Collaboration, J. Zhang, et al., Observation of $B^+ \rightarrow \rho^+ \rho^0$, Phys. Rev. Lett. 91 (2003) 221801, arXiv:hep-ex/0306007.
- [7] BaBar Collaboration, B. Aubert, et al., Measurements of branching fraction, polarization, and charge asymmetry of $B^\pm \rightarrow \rho^\pm \rho^0$ and a search for $B^\pm \rightarrow \rho^\pm f_0(980)$, Phys. Rev. Lett. 97 (2006) 261801, arXiv:hep-ex/0607092.
- [8] BaBar Collaboration, B. Aubert, et al., Measurement of the branching fraction, polarization, and CP asymmetries in $B^0 \rightarrow \rho^0 \rho^0$ decay, and implications for the CKM angle α , Phys. Rev. D 78 (2008) 071104, arXiv:0807.4977.
- [9] Belle Collaboration, P. Vanhoefer, et al., Study of $B^0 \rightarrow \rho^0 \rho^0$ decays, implications for the CKM angle ϕ_2 and search for other four pion final states, Phys. Rev. D 89 (2014) 072008, arXiv:1212.4015.
- [10] LHCb Collaboration, A.A. Alves Jr., et al., The LHCb detector at the LHC, J. Instrum. 3 (2008) 08005.
- [11] R. Aaij, et al., LHCb detector performance, Int. J. Mod. Phys. A 30 (2015) 1530022, arXiv:1412.6352, LHCb-DP-2014-002.
- [12] R. Aaij, et al., Performance of the LHCb vertex locator, J. Instrum. 9 (2014) P09007, arXiv:1405.7808.
- [13] R. Arink, et al., Performance of the LHCb outer tracker, J. Instrum. 9 (2014) P01002, arXiv:1311.3893.
- [14] M. Adinolfi, et al., Performance of the LHCb RICH detector at the LHC, Eur. Phys. J. C 73 (2013) 2431, arXiv:1211.6759.
- [15] A.A. Alves Jr., et al., Performance of the LHCb muon system, J. Instrum. 8 (2013) P02022, arXiv:1211.1346.
- [16] R. Aaij, et al., The LHCb trigger and its performance in 2011, J. Instrum. 8 (2013) P04022, arXiv:1211.3055.
- [17] V.V. Gligorov, M. Williams, Efficient, reliable and fast high-level triggering using a bonsai boosted decision tree, J. Instrum. 8 (2013) P02013, arXiv:1210.6861.
- [18] L. Breiman, J.H. Friedman, R.A. Olshen, C.J. Stone, Classification and regression trees, Wadsworth International Group, Belmont, California, USA, 1984.
- [19] R.E. Schapire, Y. Freund, A decision-theoretic generalization of on-line learning and an application to boosting, J. Comput. Syst. Sci. 55 (1997) 119.
- [20] G. Punzi, Sensitivity of searches for new signals and its optimization, in: L. Lyons, R. Mount, R. Reitmeyer (Eds.), Statistical Problems in Particle Physics, Astrophysics, and Cosmology, 2003, p. 79, arXiv:physics/0308063.
- [21] Particle Data Group, K.A. Olive, et al., Review of particle physics, Chin. Phys. C 38 (2014) 090001.
- [22] T. Sjöstrand, S. Mrenna, P. Skands, A brief introduction to PYTHIA 8.1, Comput. Phys. Commun. 178 (2008) 852, arXiv:0710.3820.
- [23] I. Belyaev, et al., Handling of the generation of primary events in Gauss, the LHCb simulation framework, in: Nuclear Science Symposium Conference Record (NSS/MIC), IEEE, 2010, p. 1155.
- [24] D.J. Lange, The EvtGen particle decay simulation package, Nucl. Instrum. Methods Phys. Res., Sect. A, Accel. Spectrom. Detect. Assoc. Equip. 462 (2001) 152.
- [25] Geant4 Collaboration, J. Allison, et al., Geant4 developments and applications, IEEE Trans. Nucl. Sci. 53 (2006) 270;
Geant4 Collaboration, S. Agostinelli, et al., Geant4: a simulation toolkit, Nucl. Instrum. Methods Phys. Res., Sect. A, Accel. Spectrom. Detect. Assoc. Equip. 506 (2003) 250.
- [26] M. Clemencic, et al., The LHCb simulation application, Gauss: design, evolution and experience, J. Phys. Conf. Ser. 331 (2011) 032023.
- [27] T. Skwarnicki, A study of the radiative cascade transitions between the Upsilon-prime and Upsilon resonances, PhD thesis, Institute of Nuclear Physics, Krakow, 1986, DESY-F31-86-02.
- [28] ARGUS Collaboration, H. Albrecht, et al., Exclusive hadronic decays of B mesons, Z. Phys. C 48 (1990) 543.
- [29] M. Pivk, F.R. Le Diberder, sPlot: a statistical tool to unfold data distributions, Nucl. Instrum. Methods Phys. Res., Sect. A, Accel. Spectrom. Detect. Assoc. Equip. 555 (2005) 356, arXiv:physics/0402083.
- [30] G.J. Gounaris, J.J. Sakurai, Finite width corrections to the vector meson dominance prediction for $\rho \rightarrow e^+ e^-$, Phys. Rev. Lett. 21 (1968) 244.
- [31] S.M. Flatté, On the nature of 0^+ mesons, Phys. Lett. B 63 (1976) 228.
- [32] S.M. Flatté, Coupled – channel analysis of the $\pi\eta$ and $K - \bar{K}$ systems near $K - \bar{K}$ threshold, Phys. Lett. B 63 (1976) 224.
- [33] S.U. Chung, et al., Partial wave analysis in k-matrix formalism, Ann. Phys. 507 (5) (1995) 404.
- [34] CLEO Collaboration, H. Muramatsu, et al., Dalitz analysis of $D^0 \rightarrow K_S^0 \pi^+ \pi^-$, Phys. Rev. Lett. 89 (2002) 251802, arXiv:hep-ex/0207067.
- [35] B. Bhattacharya, A. Datta, M. Duraisamy, D. London, Searching for new physics with bs Bs0V1V2 penguin decays, Phys. Rev. D 88 (1) (2013) 016007, arXiv:1306.1911.
- [36] M. Williams, How good are your fits? Unbinned multivariate goodness-of-fit tests in high energy physics, J. Instrum. 5 (2010) P09004, arXiv:1006.3019.
- [37] BaBar Collaboration, B. Aubert, et al., Measurement of branching fractions of B decays to $K(1)(1270)\pi$ and $K(1)(1400)\pi$ and determination of the CKM angle alpha from $B^0 \rightarrow a(1)(1260)^{\pm} \pi^{\mp}$, Phys. Rev. D 81 (2010) 052009, arXiv:0909.2171.
- [38] T. du Pree, Search for a strange phase in beautiful oscillations, CERN-THESIS-2010-124, Nikhef, Amsterdam, 2010.
- [39] Belle, J. Dalseno, et al., Measurement of branching fraction and first evidence of CP violation in $B^0 \rightarrow a_1^+(1260)\pi^+$ decays, Phys. Rev. D 86 (2012) 092012, arXiv:1205.5957.
- [40] LHCb Collaboration, R. Aaij, et al., Measurement of polarization amplitudes and CP asymmetries in $B^0 \rightarrow \phi K^*(892)^0$, J. High Energy Phys. 05 (2014) 069, arXiv:1403.2888.
- [41] L. Lyons, D. Gibaut, P. Clifford, How to combine correlated estimates of a single physical quantity, Nucl. Instrum. Methods Phys. Res., Sect. A, Accel. Spectrom. Detect. Assoc. Equip. 270 (1988) 110.
- [42] BaBar Collaboration, B. Aubert, et al., Time-dependent and time-integrated angular analysis of $B^0 \rightarrow \phi K_S \pi^0$ and $B^0 \rightarrow \phi K^+ \pi^-$, Phys. Rev. D 78 (2008) 092008, arXiv:0808.3586.
- [43] Belle Collaboration, M. Prim, et al., Angular analysis of $B^0 \rightarrow \phi K^*$ decays and search for CP violation at Belle, Phys. Rev. D 88 (7) (2013) 072004, arXiv:1308.1830.
- [44] CLEO Collaboration, R.A. Briere, et al., Observation of $B^0 \rightarrow \phi K$ and $B^0 \rightarrow \phi K^*$, Phys. Rev. Lett. 86 (2001) 3718, arXiv:hep-ex/0101032.

LHCb Collaboration

- R. Aaij ⁴¹, B. Adeva ³⁷, M. Adinolfi ⁴⁶, A. Affolder ⁵², Z. Ajaltouni ⁵, S. Akar ⁶, J. Albrecht ⁹, F. Alessio ³⁸, M. Alexander ⁵¹, S. Ali ⁴¹, G. Alkhazov ³⁰, P. Alvarez Cartelle ⁵³, A.A. Alves Jr ⁵⁷, S. Amato ², S. Amerio ²², Y. Amhis ⁷, L. An ³, L. Anderlini ^{17,g}, J. Anderson ⁴⁰, M. Andreotti ^{16,f}, J.E. Andrews ⁵⁸, R.B. Appleby ⁵⁴, O. Aquines Gutierrez ¹⁰, F. Archilli ³⁸, A. Artamonov ³⁵, M. Artuso ⁵⁹, E. Aslanides ⁶, G. Auriemma ^{25,n}, M. Baalouch ⁵, S. Bachmann ¹¹, J.J. Back ⁴⁸, A. Badalov ³⁶, C. Baesso ⁶⁰, W. Baldini ^{16,38}, R.J. Barlow ⁵⁴, C. Barschel ³⁸, S. Barsuk ⁷, W. Barter ³⁸, V. Batozskaya ²⁸, V. Battista ³⁹, A. Bay ³⁹, L. Beaucourt ⁴, J. Beddow ⁵¹, F. Bedeschi ²³, I. Bediaga ¹, L.J. Bel ⁴¹, I. Belyaev ³¹, E. Ben-Haim ⁸, G. Bencivenni ¹⁸, S. Benson ³⁸, J. Benton ⁴⁶, A. Berezhnoy ³², R. Bernet ⁴⁰, A. Bertolin ²², M.-O. Bettler ³⁸, M. van Beuzekom ⁴¹, A. Bien ¹¹, S. Bifani ⁴⁵, T. Bird ⁵⁴, A. Bizzeti ^{17,i}, T. Blake ⁴⁸, F. Blanc ³⁹, J. Blouw ¹⁰, S. Blusk ⁵⁹, V. Bocci ²⁵, A. Bondar ³⁴, N. Bondar ^{30,38}, W. Bonivento ¹⁵, S. Borghi ⁵⁴, M. Borsato ⁷, T.J.V. Bowcock ⁵², E. Bowen ⁴⁰, C. Bozzi ¹⁶, S. Braun ¹¹, D. Brett ⁵⁴, M. Britsch ¹⁰, T. Britton ⁵⁹, J. Brodzicka ⁵⁴, N.H. Brook ⁴⁶, A. Bursche ⁴⁰, J. Buytaert ³⁸, S. Cadeddu ¹⁵, R. Calabrese ^{16,f}, M. Calvi ^{20,k}, M. Calvo Gomez ^{36,p}, P. Campana ¹⁸, D. Campora Perez ³⁸, L. Capriotti ⁵⁴, A. Carbone ^{14,d}, G. Carboni ^{24,l}, R. Cardinale ^{19,j}, A. Cardini ¹⁵, P. Carniti ²⁰, L. Carson ⁵⁰, K. Carvalho Akiba ^{2,38}, R. Casanova Mohr ³⁶, G. Can ⁵², L. Cassina ^{20,k}, L. Castillo Garcia ³⁸, M. Cattaneo ³⁸, Ch. Cauet ⁹, G. Cavallero ¹⁹, R. Cenci ^{23,t}, M. Charles ⁸, Ph. Charpentier ³⁸, M. Chefdeville ⁴, S. Chen ⁵⁴, S.-F. Cheung ⁵⁵, N. Chiapolini ⁴⁰, M. Chrzaszcz ^{40,26}, X. Cid Vidal ³⁸, G. Ciezarek ⁴¹, P.E.L. Clarke ⁵⁰, M. Clemencic ³⁸, H.V. Cliff ⁴⁷, J. Closier ³⁸, V. Coco ³⁸, J. Cogan ⁶, E. Cogneras ⁵, V. Cogoni ^{15,e}, L. Cojocariu ²⁹, G. Collazuol ²², P. Collins ³⁸, A. Comerma-Montells ¹¹, A. Contu ^{15,38}, A. Cook ⁴⁶, M. Coombes ⁴⁶, S. Coquereau ⁸, G. Corti ³⁸, M. Corvo ^{16,f}, I. Counts ⁵⁶, B. Couturier ³⁸, G.A. Cowan ⁵⁰, D.C. Craik ⁴⁸, A.C. Crocombe ⁴⁸, M. Cruz Torres ⁶⁰, S. Cunliffe ⁵³, R. Currie ⁵³, C. D'Ambrosio ³⁸, J. Dalseno ⁴⁶, P.N.Y. David ⁴¹, A. Davis ⁵⁷, K. De Bruyn ⁴¹, S. De Capua ⁵⁴, M. De Cian ¹¹, J.M. De Miranda ¹, L. De Paula ², W. De Silva ⁵⁷, P. De Simone ¹⁸, C.-T. Dean ⁵¹, D. Decamp ⁴, M. Deckenhoff ⁹, L. Del Buono ⁸, N. Déléage ⁴, D. Derkach ⁵⁵, O. Deschamps ⁵, F. Dettori ³⁸, B. Dey ⁴⁰, A. Di Canto ³⁸, F. Di Ruscio ²⁴, H. Dijkstra ³⁸, S. Donleavy ⁵², F. Dordei ¹¹, M. Dorigo ³⁹, A. Dosil Suárez ³⁷, D. Dossett ⁴⁸, A. Dovbnya ⁴³, K. Dreimanis ⁵², G. Dujany ⁵⁴, F. Dupertuis ³⁹, P. Durante ³⁸, R. Dzhelyadin ³⁵, A. Dziurda ²⁶, A. Dzyuba ³⁰, S. Easo ^{49,38}, U. Egede ⁵³, V. Egorychev ³¹, S. Eidelman ³⁴, S. Eisenhardt ⁵⁰, U. Eitschberger ⁹, R. Ekelhof ⁹, L. Eklund ⁵¹, I. El Rifai ⁵, Ch. Elsasser ⁴⁰, S. Ely ⁵⁹, S. Esen ¹¹, H.M. Evans ⁴⁷, T. Evans ⁵⁵, A. Falabella ¹⁴, C. Färber ¹¹, C. Farinelli ⁴¹, N. Farley ⁴⁵, S. Farry ⁵², R. Fay ⁵², D. Ferguson ⁵⁰, V. Fernandez Albor ³⁷, F. Ferrari ¹⁴, F. Ferreira Rodrigues ¹, M. Ferro-Luzzi ³⁸, S. Filippov ³³, M. Fiore ^{16,38,f}, M. Fiorini ^{16,f}, M. Firlej ²⁷, C. Fitzpatrick ³⁹, T. Fiutowski ²⁷, P. Fol ⁵³, M. Fontana ¹⁰, F. Fontanelli ^{19,j}, R. Forty ³⁸, O. Francisco ², M. Frank ³⁸, C. Frei ³⁸, M. Frosini ¹⁷, J. Fu ^{21,38}, E. Furfarò ^{24,l}, A. Gallas Torreira ³⁷, D. Galli ^{14,d}, S. Gallorini ^{22,38}, S. Gambetta ^{19,j}, M. Gandelman ², P. Gandini ⁵⁵, Y. Gao ³, J. García Pardiñas ³⁷, J. Garofoli ⁵⁹, J. Garra Tico ⁴⁷, L. Garrido ³⁶, D. Gascon ³⁶, C. Gaspar ³⁸, U. Gastaldi ¹⁶, R. Gauld ⁵⁵, L. Gavardi ⁹, G. Gazzoni ⁵, A. Geraci ^{21,v}, D. Gerick ¹¹, E. Gersabeck ¹¹, M. Gersabeck ⁵⁴, T. Gershon ⁴⁸, Ph. Ghez ⁴, A. Gianelle ²², S. Gianì ³⁹, V. Gibson ⁴⁷, L. Giubega ²⁹, V.V. Gligorov ³⁸, C. Göbel ⁶⁰, D. Golubkov ³¹, A. Golutvin ^{53,31,38}, A. Gomes ^{1,a}, C. Gotti ^{20,k}, M. Grabalosa Gándara ^{5,*}, R. Graciani Diaz ³⁶, L.A. Granado Cardoso ³⁸, E. Graugés ³⁶, E. Graverini ⁴⁰, G. Graziani ¹⁷, A. Grecu ²⁹, E. Greening ⁵⁵, S. Gregson ⁴⁷, P. Griffith ⁴⁵, L. Grillo ¹¹, O. Grünewberg ⁶³, B. Gui ⁵⁹, E. Gushchin ³³, Yu. Guz ^{35,38}, T. Gys ³⁸, C. Hadjivasiliou ⁵⁹, G. Haefeli ³⁹, C. Haen ³⁸, S.C. Haines ⁴⁷, S. Hall ⁵³, B. Hamilton ⁵⁸, T. Hampson ⁴⁶, X. Han ¹¹, S. Hansmann-Menzemer ¹¹, N. Harnew ⁵⁵, S.T. Harnew ⁴⁶, J. Harrison ⁵⁴, J. He ³⁸, T. Head ³⁹, V. Heijne ⁴¹, K. Hennessy ⁵², P. Henrard ⁵, L. Henry ⁸, J.A. Hernando Morata ³⁷, E. van Herwijnen ³⁸, M. Heß ⁶³, A. Hicheur ², D. Hill ⁵⁵, M. Hoballah ⁵, C. Hombach ⁵⁴, W. Hulsbergen ⁴¹, T. Humair ⁵³, N. Hussain ⁵⁵, D. Hutchcroft ⁵², D. Hynds ⁵¹, M. Idzik ²⁷, P. Ilten ⁵⁶, R. Jacobsson ³⁸, A. Jaeger ¹¹, J. Jalocha ⁵⁵, E. Jans ⁴¹, A. Jawahery ⁵⁸, F. Jing ³, M. John ⁵⁵, D. Johnson ³⁸, C.R. Jones ⁴⁷, C. Joram ³⁸, B. Jost ³⁸, N. Jurik ⁵⁹, S. Kandybei ⁴³, W. Kanso ⁶, M. Karacson ³⁸, T.M. Karbach ³⁸, S. Karodia ⁵¹, M. Kelsey ⁵⁹, I.R. Kenyon ⁴⁵, M. Kenzie ³⁸, T. Ketel ⁴², B. Khanji ^{20,38,k}, C. Khurewathanakul ³⁹, S. Klaver ⁵⁴, K. Klimaszewski ²⁸, O. Kochebina ⁷, M. Kolpin ¹¹, I. Komarov ³⁹, R.F. Koopman ⁴², P. Koppenburg ^{41,38}, M. Korolev ³², L. Kravchuk ³³, K. Kreplin ¹¹, M. Kreps ⁴⁸, G. Krocker ¹¹, P. Krokovny ³⁴, F. Kruse ⁹, W. Kucewicz ^{26,o}, M. Kucharczyk ²⁶, V. Kudryavtsev ³⁴, K. Kurek ²⁸, T. Kvaratskheliya ³¹, V.N. La Thi ³⁹, D. Lacarrere ³⁸, G. Lafferty ⁵⁴, A. Lai ¹⁵, D. Lambert ⁵⁰,

- R.W. Lambert ⁴², G. Lanfranchi ¹⁸, C. Langenbruch ⁴⁸, B. Langhans ³⁸, T. Latham ⁴⁸, C. Lazzeroni ⁴⁵,
 R. Le Gac ⁶, J. van Leerdam ⁴¹, J.-P. Lees ⁴, R. Lefèvre ⁵, A. Leflat ³², J. Lefrançois ⁷, O. Leroy ⁶, T. Lesiak ²⁶,
 B. Leverington ¹¹, Y. Li ⁷, T. Likhomanenko ⁶⁴, M. Liles ⁵², R. Lindner ³⁸, C. Linn ³⁸, F. Lionetto ⁴⁰, B. Liu ¹⁵,
 S. Lohn ³⁸, I. Longstaff ⁵¹, J.H. Lopes ², P. Lowdon ⁴⁰, D. Lucchesi ^{22,r}, H. Luo ⁵⁰, A. Lupato ²², E. Luppi ^{16,f},
 O. Lupton ⁵⁵, F. Machefert ⁷, F. Maciuc ²⁹, O. Maev ³⁰, S. Malde ⁵⁵, A. Malinin ⁶⁴, G. Manca ^{15,e},
 G. Mancinelli ⁶, P. Manning ⁵⁹, A. Mapelli ³⁸, J. Maratas ⁵, J.F. Marchand ⁴, U. Marconi ¹⁴,
 C. Marin Benito ³⁶, P. Marino ^{23,38,t}, R. Märki ³⁹, J. Marks ¹¹, G. Martellotti ²⁵, M. Martinelli ³⁹,
 D. Martinez Santos ⁴², F. Martinez Vidal ⁶⁶, D. Martins Tostes ², A. Massafferri ¹, R. Matev ³⁸, A. Mathad ⁴⁸,
 Z. Mathe ³⁸, C. Matteuzzi ²⁰, A. Mauri ⁴⁰, B. Maurin ³⁹, A. Mazurov ⁴⁵, M. McCann ⁵³, J. McCarthy ⁴⁵,
 A. McNab ⁵⁴, R. McNulty ¹², B. Meadows ⁵⁷, F. Meier ⁹, M. Meissner ¹¹, M. Merk ⁴¹, D.A. Milanes ⁶²,
 M.-N. Minard ⁴, D.S. Mitzel ¹¹, J. Molina Rodriguez ⁶⁰, S. Monteil ⁵, M. Morandin ²², P. Morawski ²⁷,
 A. Mordà ⁶, M.J. Morello ^{23,t}, J. Moron ²⁷, A.-B. Morris ⁵⁰, R. Mountain ⁵⁹, F. Muheim ⁵⁰, K. Müller ⁴⁰,
 M. Mussini ¹⁴, B. Muster ³⁹, P. Naik ⁴⁶, T. Nakada ³⁹, R. Nandakumar ⁴⁹, I. Nasteva ², M. Needham ⁵⁰,
 N. Neri ²¹, S. Neubert ¹¹, N. Neufeld ³⁸, M. Neuner ¹¹, A.D. Nguyen ³⁹, T.D. Nguyen ³⁹, C. Nguyen-Mau ^{39,q},
 V. Niess ⁵, R. Niet ⁹, N. Nikitin ³², T. Nikodem ¹¹, A. Novoselov ³⁵, D.P. O'Hanlon ⁴⁸,
 A. Oblakowska-Mucha ²⁷, V. Obraztsov ³⁵, S. Ogilvy ⁵¹, O. Okhrimenko ⁴⁴, R. Oldeman ^{15,e},
 C.J.G. Onderwater ⁶⁷, B. Osorio Rodrigues ¹, J.M. Otalora Goicochea ², A. Otto ³⁸, P. Owen ⁵³,
 A. Oyanguren ⁶⁶, A. Palano ^{13,c}, F. Palombo ^{21,u}, M. Palutan ¹⁸, J. Panman ³⁸, A. Papanestis ⁴⁹,
 M. Pappagallo ⁵¹, L.I. Pappalardo ^{16,f}, C. Parkes ⁵⁴, G. Passaleva ¹⁷, G.D. Patel ⁵², M. Patel ⁵³,
 C. Patrignani ^{19,j}, A. Pearce ^{54,49}, A. Pellegrino ⁴¹, G. Penso ^{25,m}, M. Pepe Altarelli ³⁸, S. Perazzini ^{14,d},
 P. Perret ⁵, L. Pescatore ⁴⁵, K. Petridis ⁴⁶, A. Petrolini ^{19,j}, E. Picatoste Olloqui ³⁶, B. Pietrzyk ⁴, T. Pilař ⁴⁸,
 D. Pinci ²⁵, A. Pistone ¹⁹, S. Playfer ⁵⁰, M. Plo Casasus ³⁷, T. Poikela ³⁸, F. Polci ⁸, A. Poluektov ^{48,34},
 I. Polyakov ³¹, E. Polycarpo ², A. Popov ³⁵, D. Popov ¹⁰, B. Popovici ²⁹, C. Potterat ², E. Price ⁴⁶, J.D. Price ⁵²,
 J. Prisciandaro ³⁹, A. Pritchard ⁵², C. Prouve ⁴⁶, V. Pugatch ⁴⁴, A. Puig Navarro ³⁹, G. Punzi ^{23,s}, W. Qian ⁴,
 R. Quagliani ^{7,46}, B. Rachwal ²⁶, J.H. Rademacker ⁴⁶, B. Rakotomiaramanana ³⁹, M. Rama ²³, M.S. Rangel ²,
 I. Raniuk ⁴³, N. Rauschmayr ³⁸, G. Raven ⁴², F. Redi ⁵³, S. Reichert ⁵⁴, M.M. Reid ⁴⁸, A.C. dos Reis ¹,
 S. Ricciardi ⁴⁹, S. Richards ⁴⁶, M. Rihl ³⁸, K. Rinnert ⁵², V. Rives Molina ³⁶, P. Robbe ^{7,38}, A.B. Rodrigues ¹,
 E. Rodrigues ⁵⁴, J.A. Rodriguez Lopez ⁶², P. Rodriguez Perez ⁵⁴, S. Roiser ³⁸, V. Romanovsky ³⁵,
 A. Romero Vidal ^{37,*}, M. Rotondo ²², J. Rouvinet ³⁹, T. Ruf ³⁸, H. Ruiz ³⁶, P. Ruiz Valls ⁶⁶,
 J.J. Saborido Silva ³⁷, N. Sagidova ³⁰, P. Sail ⁵¹, B. Saitta ^{15,e}, V. Salustino Guimaraes ²,
 C. Sanchez Mayordomo ⁶⁶, B. Sanmartin Sedes ³⁷, R. Santacesaria ²⁵, C. Santamarina Rios ³⁷,
 E. Santovetti ^{24,l}, A. Sarti ^{18,m}, C. Satriano ^{25,n}, A. Satta ²⁴, D.M. Saunders ⁴⁶, D. Savrina ^{31,32}, M. Schiller ³⁸,
 H. Schindler ³⁸, M. Schlupp ⁹, M. Schmelling ¹⁰, B. Schmidt ³⁸, O. Schneider ³⁹, A. Schopper ³⁸,
 M.-H. Schune ⁷, R. Schwemmer ³⁸, B. Sciascia ¹⁸, A. Sciubba ^{25,m}, A. Semennikov ³¹, I. Sepp ⁵³, N. Serra ⁴⁰,
 J. Serrano ⁶, L. Sestini ²², P. Seyfert ¹¹, M. Shapkin ³⁵, I. Shapoval ^{16,43,f}, Y. Shcheglov ³⁰, T. Shears ⁵²,
 L. Shekhtman ³⁴, V. Shevchenko ⁶⁴, A. Shires ⁹, R. Silva Coutinho ⁴⁸, G. Simi ²², M. Sirendi ⁴⁷,
 N. Skidmore ⁴⁶, I. Skillicorn ⁵¹, T. Skwarnicki ⁵⁹, N.A. Smith ⁵², E. Smith ^{55,49}, E. Smith ⁵³, J. Smith ⁴⁷,
 M. Smith ⁵⁴, H. Snoek ⁴¹, M.D. Sokoloff ^{57,38}, F.J.P. Soler ⁵¹, F. Soomro ³⁹, D. Souza ⁴⁶, B. Souza De Paula ²,
 B. Spaan ⁹, P. Spradlin ⁵¹, S. Sridharan ³⁸, F. Stagni ³⁸, M. Stahl ¹¹, S. Stahl ³⁸, O. Steinkamp ⁴⁰,
 O. Stenyakin ³⁵, F. Sterpka ⁵⁹, S. Stevenson ⁵⁵, S. Stoica ²⁹, S. Stone ⁵⁹, B. Storaci ⁴⁰, S. Stracka ^{23,t},
 M. Straticiuc ²⁹, U. Straumann ⁴⁰, R. Stroili ²², L. Sun ⁵⁷, W. Sutcliffe ⁵³, K. Swientek ²⁷, S. Swientek ⁹,
 V. Syropoulos ⁴², M. Szczekowski ²⁸, P. Szczypka ^{39,38}, T. Szumlak ²⁷, S. T'Jampens ⁴, M. Teklishyn ⁷,
 G. Tellarini ^{16,f}, F. Teubert ³⁸, C. Thomas ⁵⁵, E. Thomas ³⁸, J. van Tilburg ⁴¹, V. Tisserand ⁴, M. Tobin ³⁹,
 J. Todd ⁵⁷, S. Tolk ⁴², L. Tomassetti ^{16,f}, D. Tonelli ³⁸, S. Topp-Joergensen ⁵⁵, N. Torr ⁵⁵, E. Tournefier ⁴,
 S. Tourneur ³⁹, K. Trabelsi ³⁹, M.T. Tran ³⁹, M. Tresch ⁴⁰, A. Trisovic ³⁸, A. Tsaregorodtsev ⁶, P. Tsopelas ⁴¹,
 N. Tuning ^{41,38}, A. Ukleja ²⁸, A. Ustyuzhanin ⁶⁵, U. Uwer ¹¹, C. Vacca ^{15,e}, V. Vagnoni ¹⁴, G. Valenti ¹⁴,
 A. Vallier ⁷, R. Vazquez Gomez ¹⁸, P. Vazquez Regueiro ³⁷, C. Vázquez Sierra ³⁷, S. Vecchi ¹⁶, J.J. Velthuis ⁴⁶,
 M. Veltri ^{17,h}, G. Veneziano ³⁹, M. Vesterinen ¹¹, J.V. Viana Barbosa ³⁸, B. Viaud ⁷, D. Vieira ²,
 M. Vieites Diaz ³⁷, X. Vilasis-Cardona ^{36,p}, A. Vollhardt ⁴⁰, D. Volyansky ¹⁰, D. Voong ⁴⁶, A. Vorobyev ³⁰,
 V. Vorobyev ³⁴, C. Voß ⁶³, J.A. de Vries ⁴¹, R. Waldi ⁶³, C. Wallace ⁴⁸, R. Wallace ¹², J. Walsh ²³,
 S. Wandernoth ¹¹, J. Wang ⁵⁹, D.R. Ward ⁴⁷, N.K. Watson ⁴⁵, D. Websdale ⁵³, A. Weiden ⁴⁰,
 M. Whitehead ⁴⁸, D. Wiedner ¹¹, G. Wilkinson ^{55,38}, M. Wilkinson ⁵⁹, M. Williams ³⁸, M.P. Williams ⁴⁵,

M. Williams⁵⁶, F.F. Wilson⁴⁹, J. Wimberley⁵⁸, J. Wishahi⁹, W. Wislicki²⁸, M. Witek²⁶, G. Wormser⁷, S.A. Wotton⁴⁷, S. Wright⁴⁷, K. Wyllie³⁸, Y. Xie⁶¹, Z. Xu³⁹, Z. Yang³, X. Yuan³⁴, O. Yushchenko³⁵, M. Zangoli¹⁴, M. Zavertyaev^{10,b}, L. Zhang³, Y. Zhang³, A. Zhelezov¹¹, A. Zhokhov³¹, L. Zhong³

¹ Centro Brasileiro de Pesquisas Físicas (CBPF), Rio de Janeiro, Brazil

² Universidade Federal do Rio de Janeiro (UFRJ), Rio de Janeiro, Brazil

³ Center for High Energy Physics, Tsinghua University, Beijing, China

⁴ LAPP, Université Savoie Mont-Blanc, CNRS/IN2P3, Annecy-Le-Vieux, France

⁵ Clermont Université, Université Blaise Pascal, CNRS/IN2P3, LPC, Clermont-Ferrand, France

⁶ CPPM, Aix-Marseille Université, CNRS/IN2P3, Marseille, France

⁷ LAL, Université Paris-Sud, CNRS/IN2P3, Orsay, France

⁸ LPNHE, Université Pierre et Marie Curie, Université Paris Diderot, CNRS/IN2P3, Paris, France

⁹ Fakultät Physik, Technische Universität Dortmund, Dortmund, Germany

¹⁰ Max-Planck-Institut für Kernphysik (MPIK), Heidelberg, Germany

¹¹ Physikalisches Institut, Ruprecht-Karls-Universität Heidelberg, Heidelberg, Germany

¹² School of Physics, University College Dublin, Dublin, Ireland

¹³ Sezione INFN di Bari, Bari, Italy

¹⁴ Sezione INFN di Bologna, Bologna, Italy

¹⁵ Sezione INFN di Cagliari, Cagliari, Italy

¹⁶ Sezione INFN di Ferrara, Ferrara, Italy

¹⁷ Sezione INFN di Firenze, Firenze, Italy

¹⁸ Laboratori Nazionali dell'INFN di Frascati, Frascati, Italy

¹⁹ Sezione INFN di Genova, Genova, Italy

²⁰ Sezione INFN di Milano Bicocca, Milano, Italy

²¹ Sezione INFN di Milano, Milano, Italy

²² Sezione INFN di Padova, Padova, Italy

²³ Sezione INFN di Pisa, Pisa, Italy

²⁴ Sezione INFN di Roma Tor Vergata, Roma, Italy

²⁵ Sezione INFN di Roma La Sapienza, Roma, Italy

²⁶ Henryk Niewodniczanski Institute of Nuclear Physics Polish Academy of Sciences, Kraków, Poland

²⁷ AGH – University of Science and Technology, Faculty of Physics and Applied Computer Science, Kraków, Poland

²⁸ National Center for Nuclear Research (NCBJ), Warsaw, Poland

²⁹ Horia Hulubei National Institute of Physics and Nuclear Engineering, Bucharest-Magurele, Romania

³⁰ Petersburg Nuclear Physics Institute (PNPI), Gatchina, Russia

³¹ Institute of Theoretical and Experimental Physics (ITEP), Moscow, Russia

³² Institute of Nuclear Physics, Moscow State University (SINP MSU), Moscow, Russia

³³ Institute for Nuclear Research of the Russian Academy of Sciences (INR RAN), Moscow, Russia

³⁴ Budker Institute of Nuclear Physics (SB RAS) and Novosibirsk State University, Novosibirsk, Russia

³⁵ Institute for High Energy Physics (IHEP), Protvino, Russia

³⁶ Universitat de Barcelona, Barcelona, Spain

³⁷ Universidad de Santiago de Compostela, Santiago de Compostela, Spain

³⁸ European Organization for Nuclear Research (CERN), Geneva, Switzerland

³⁹ Ecole Polytechnique Fédérale de Lausanne (EPFL), Lausanne, Switzerland

⁴⁰ Physik-Institut, Universität Zürich, Zürich, Switzerland

⁴¹ Nikhef National Institute for Subatomic Physics, Amsterdam, The Netherlands

⁴² Nikhef National Institute for Subatomic Physics and VU University Amsterdam, Amsterdam, The Netherlands

⁴³ NSC Kharkiv Institute of Physics and Technology (NSC KIPT), Kharkiv, Ukraine

⁴⁴ Institute for Nuclear Research of the National Academy of Sciences (KINR), Kyiv, Ukraine

⁴⁵ University of Birmingham, Birmingham, United Kingdom

⁴⁶ H.H. Wills Physics Laboratory, University of Bristol, Bristol, United Kingdom

⁴⁷ Cavendish Laboratory, University of Cambridge, Cambridge, United Kingdom

⁴⁸ Department of Physics, University of Warwick, Coventry, United Kingdom

⁴⁹ STFC Rutherford Appleton Laboratory, Didcot, United Kingdom

⁵⁰ School of Physics and Astronomy, University of Edinburgh, Edinburgh, United Kingdom

⁵¹ School of Physics and Astronomy, University of Glasgow, Glasgow, United Kingdom

⁵² Oliver Lodge Laboratory, University of Liverpool, Liverpool, United Kingdom

⁵³ Imperial College London, London, United Kingdom

⁵⁴ School of Physics and Astronomy, University of Manchester, Manchester, United Kingdom

⁵⁵ Department of Physics, University of Oxford, Oxford, United Kingdom

⁵⁶ Massachusetts Institute of Technology, Cambridge, MA, United States

⁵⁷ University of Cincinnati, Cincinnati, OH, United States

⁵⁸ University of Maryland, College Park, MD, United States

⁵⁹ Syracuse University, Syracuse, NY, United States

⁶⁰ Pontifícia Universidade Católica do Rio de Janeiro (PUC-Rio), Rio de Janeiro, Brazil^w

⁶¹ Institute of Particle Physics, Central China Normal University, Wuhan, Hubei, China^x

⁶² Departamento de Física, Universidad Nacional de Colombia, Bogota, Colombia^y

⁶³ Institut für Physik, Universität Rostock, Rostock, Germany^z

⁶⁴ National Research Centre Kurchatov Institute, Moscow, Russia^{aa}

⁶⁵ Yandex School of Data Analysis, Moscow, Russia^{aa}

⁶⁶ Instituto de Física Corpuscular (IFIC), Universitat de València-CSIC, Valencia, Spain^{ab}

⁶⁷ Van Swinderen Institute, University of Groningen, Groningen, The Netherlands^{ac}

* Corresponding author.

E-mail address: mgrabalo@cern.ch (M. Grabalosa Gándara).

^a Universidade Federal do Triângulo Mineiro (UFTM), Uberaba-MG, Brazil.

^b P.N. Lebedev Physical Institute, Russian Academy of Science (LPI RAS), Moscow, Russia.

^c Università di Bari, Bari, Italy.

- ^d Università di Bologna, Bologna, Italy.
^e Università di Cagliari, Cagliari, Italy.
^f Università di Ferrara, Ferrara, Italy.
^g Università di Firenze, Firenze, Italy.
^h Università di Urbino, Urbino, Italy.
ⁱ Università di Modena e Reggio Emilia, Modena, Italy.
^j Università di Genova, Genova, Italy.
^k Università di Milano Bicocca, Milano, Italy.
^l Università di Roma Tor Vergata, Roma, Italy.
^m Università di Roma La Sapienza, Roma, Italy.
ⁿ Università della Basilicata, Potenza, Italy.
^o AGH – University of Science and Technology, Faculty of Computer Science, Electronics and Telecommunications, Kraków, Poland.
^p LIFAELS, La Salle, Universitat Ramon Llull, Barcelona, Spain.
^q Hanoi University of Science, Hanoi, Viet Nam.
^r Università di Padova, Padova, Italy.
^s Università di Pisa, Pisa, Italy.
^t Scuola Normale Superiore, Pisa, Italy.
^u Università degli Studi di Milano, Milano, Italy.
^v Politecnico di Milano, Milano, Italy.
^w Associated to: Universidade Federal do Rio de Janeiro (UFRJ), Rio de Janeiro, Brazil.
^x Associated to: Center for High Energy Physics, Tsinghua University, Beijing, China.
^y Associated to: LPNHE, Université Pierre et Marie Curie, Université Paris Diderot, CNRS/IN2P3, Paris, France.
^z Associated to: Physikalisches Institut, Ruprecht-Karls-Universität Heidelberg, Heidelberg, Germany.
^{aa} Associated to: Institute of Theoretical and Experimental Physics (ITEP), Moscow, Russia.
^{ab} Associated to: Universitat de Barcelona, Barcelona, Spain.
^{ac} Associated to: Nikhef National Institute for Subatomic Physics, Amsterdam, The Netherlands.